Chinese Chemical Letters 34 (2023) 107501

Contents lists available at ScienceDirect

Chinese Chemical Letters

journal homepage: www.elsevier.com/locate/cclet

Emerging multifunctional iron-based nanomaterials as polysulfides adsorbent and sulfur species catalyst for lithium-sulfur batteries—A mini-review

Xinxing Sun, Shuangke Liu*, Weiwei Sun*, Chunman Zheng*

College of Aerospace Science and Engineering, National University of Defense Technology, Changsha 410073, China

ARTICLE INFO

Article history:
Received 19 January 2022
Revised 3 April 2022
Accepted 7 May 2022
Available online 11 May 2022

Keywords:
Iron-based nanomaterials
Polysulfides
Chemical anchoring
Electrocatalyst
Lithium-sulfur batteries

ABSTRACT

Lithium-sulfur (Li-S) battery has been considered as one of the most promising next generation energy storage technologies for its overwhelming merits of high theoretical specific capacity (1673 mAh/g), high energy density (2500 Wh/kg), low cost, and environmentally friendliness of sulfur. However, critical drawbacks, including inherent low conductivity of sulfur and Li_2S, large volume changes of sulfur cathodes, undesirable shuttling and sluggish redox kinetics of polysulfides, seriously deteriorate the energy density, cycle life and rate capability of Li-S battery, and thus limit its practical applications. Herein, we reviewed the recent developments addressing these problems through iron-based nanomaterials for effective synergistic immobilization as well as conversion reaction kinetics acceleration for polysulfides. The mechanist configurations between different iron-based nanomaterials and polysulfides for entrapment and conversion acceleration were summarized at first. Then we concluded the recent progresses on utilizing various iron-based nanomaterials in Li-S battery as sulfur hosts, separators and cathode interlayers. Finally, we discussed the challenges and perspectives for designing high sulfur loading cathode architectures along with outstanding chemisorption capability and catalytic activity.

© 2022 Published by Elsevier B.V. on behalf of Chinese Chemical Society and Institute of Materia Medica, Chinese Academy of Medical Sciences.

1. Introduction

As a dominant type of secondary batteries in the energy storage market, lithium-ion battery (LIB), based on lithium intercalation electrochemistry, has experienced a prosperous development and growth over the last few decades, from hand-held electronic devices to all-electric vehicles and even micro/mini smart grids, almost covering all the aspects concerning to our lives. However, Li-ion battery will eventually meet its density limits (merely 400 Wh/kg under ideal conditions) with the advancement of energy storage demand within next 10 years [1,2]. Therefore, a battery chemistry with a higher energy storage capability at a reasonable cost is expected. Out of the state-of-the-art energy storage technologies, lithium-sulfur (Li-S) battery, of which the constitute parts are displayed in Fig. 1a has been considered as one of the most promising candidates to fulfill the forthcoming energy requirements for its overwhelming merits, including ultrahigh theoretical capacity (1672 mAh/g) and theoretical energy density (2500 Wh/kg) [3], which is almost an order of magnitude higher than that of commercial LIBs (Fig. 1b) [4], and cost-effectiveness as well as natural abundance of sulfur species.

Different from LIBs, the reaction mechanism of Li-S batteries involves a multiple-electron transfer process, which can be divided into three stages approximately as shown in Fig. 1c [5]: (1) $S_8 + 2e^- + 2Li^+ \rightarrow Li_2S_8$; (2) $Li_2S_8 + 2/3e^- + 2/3Li^+ \rightarrow 4/3Li_2S_6$; $Li_2S_6 + e^- + Li^+ \rightarrow 3/2Li_2S_4$; and (3) $Li_2S_4 + 2e^- + 2Li^+ \rightarrow 2Li_2S_2$; $Li_2S_2 + 2e^- + 2Li^+ \rightarrow 2Li_2S$. Notably, the reaction rate constants of processes from long-chain Li_2S_8 to short-chain Li_2S_4 and to Li_2S_2 are 0.368 h^{-1} and 0.276 h^{-1}, respectively. In comparison, the reaction rate constant of the process from Li_2S_2 to Li_2S reaches only 0.061 h^{-1}, which can be ascribed to the intrinsic nature of the solid-solid conversion reaction, indicating that the reaction rate of sulfur conversion is predominantly controlled by the last solid-solid process [6]. Unfortunately, to achieve the practical application of Li-S battery, there is still a long way to go, which is mainly plagued by several obstacles [7,8]. One is the insulting nature of sulfur and lithium sulfides, which limits the continuous conduction of cathode, thus leading to sluggish dynamics and insufficient performance of active materials. Second, the intermediate lithium polysulfides (LiPSs) are highly soluble in the electrolyte, which shuttle back and forth between the cathode and anode (so-called "shuttle effect") and react with lithium metal to produce

* Corresponding authors.
E-mail addresses: liu_sk@139.com (S. Liu), wwsun@nudt.edu.cn (W. Sun), zhengchunman@nudt.edu.cn (C. Zheng).

https://doi.org/10.1016/j.cclet.2022.05.015
1001-8417/© 2022 Published by Elsevier B.V. on behalf of Chinese Chemical Society and Institute of Materia Medica, Chinese Academy of Medical Sciences.

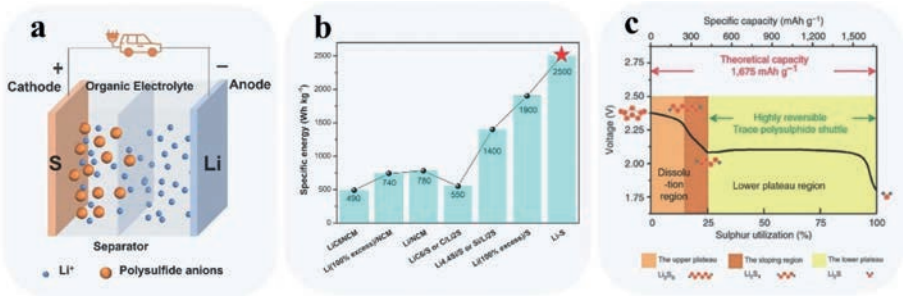

Fig. 1. (a) A schematic diagram of a Li-S battery. (b) Specific energies of alternative technologies for LIBs. Reproduced with permission [4]. Copyright 2021, The Royal Society of Chemistry. (c) The discharge curve correlated to reaction mechanism of Li-S battery. Reproduced with permission [5]. Copyright 2013, Nature Publishing Group.

irreversible products which deposited on the anode surface, resulting in an irreversible loss of active substrates and increasing internal resistance which led to sluggish kinetics of LiPSs conversion reaction consequently. Third, the undesirable volume fluctuation of sulfur during charge and discharge process since the grant difference in density between S_8 (2.07 g/cm^3) and Li_2S (1.66 g/cm^3). Last but not least, the uncontrollable lithium dendrites grow on the anode surface owing to the repeated dissolution of lithium (stripping process) and its heterogeneous deposition on the anode (platting process).

To address the above-mentioned critical issues, enormous efforts have been dedicated towards different components of Li-S battery to promote the electrochemical performances, including multifunctional cathodes [9], modified separators [10], intermediate interlayers [11] and additive electrolytes [12], *etc.* Among these sundry optimization methods, the most studied and effective measurement is to construct a multifunctional cathode. With the developing understanding about Li-S battery system, the construction strategy of cathode can be divided into three stages.

At the first stage, various carbon-based materials with elaborately designed porous structures and interconnected networks such as graphene sheets, porous carbon, carbon spheres or nanotubes, are designed and adopted to accommodate sulfur for enhanced battery performances. For instance, these carbon matrix materials, usually with good compatibility for sulfur and excellent conductivity of electrons and ions, are designed to provide abundant sulfur loading space and physical confinement for polysulfides.

However, the weak interaction between the non-polar carbonaceous matrix and polar polysulfides cannot suppress the shuttle effect effectively over long-term cycling, leading to severe capacity degradation irresistibly. In order to enhance the chemisorption ability of carbon host, heteroatoms [4] and intrinsic defect [13] are introduced in carbon matrix to offer active sites with polar bonds for the second stage. The doped atoms contain metal atoms (Fe, Co and Ni, *etc.*) and non-metal atoms (N, P, S and B, *etc.*), which exhibit strengthened capability to immobilize polysulfides to an extent. Nevertheless, their electrochemical performances are still insufficient to afford large-scale utilization because of the finiteness of the adsorption sites and the sluggish reaction kinetics.

For the third stage, researchers found sulfur host materials that feature both chemical adsorption and electrocatalytic capabilities for LiPS species more effectively to solve the above problems of sulfur cathode [14]. The polar metals (Pt, Ag, *etc.*) and transition metal compounds (oxides, nitrides, sulfides, phosphides, borides, hydroxides, *etc.*) catalysts could accelerate the conversion reaction of anchored LiPSs as well as suppress the shuttling effect for strong chemical adsorptions which is favorable for developing practically useable Li-S battery [15]. Avara *et al.* [16,17] first studied the electrocatalytic effects of noble metal Pt towards the polysulfides redox reactions in the early days and found that the Pt nanocrystals can promote the conversion of Li_2S_2 or Li_2S to long-chain polysulfides effectively, and mitigate the agglomeration of active substances on the electrode during cycling. In order to explore more scalable metal catalysts, numerous transition metals and their compounds have been introduced into Li-S battery system for catalyzing the redox reactions of LiPSs, as well as supplying with stronger chemical bonding forces towards polar polysulfides, such as Ti-based [18], Fe-based [19], Co-based [20], Ni-based [21].

Among these common metal elements, Fe-, Co- and Ni-based compounds [14,22] attracted most attentions because they belong to the VIII family in the periodic table, and have excellent catalytic properties due to the unfilled d orbital in valence electrons. In addition, due to the natural abundance, low cost, good biocompatibility, non-toxicity and catalytic activity of iron, Fe-based electrocatalysts have attracted researchers' interests in many fields such as conversion of CO_2 to CO [23], oxygen reduction reaction [24], as well as energy storage systems like sodium-ion battery [25], potassium-ion battery [26], lithium-ion battery [27] and lithium-sulfur battery [28]. The uniqueness of electronic structure and low field splitting energy of iron atoms which benefit the formation of various iron-based compounds effortlessly have granted the prosperous development of iron-based materials. Besides, the characteristics of rich raw materials, low cost and environmental friendliness of iron-based electrocatalysts favors their large-scale application compared with other transitional metal catalysts, such as Co- and Ni-based compounds [20,29,30].

In recent years, a massive number of iron-based nanomaterials with extraordinary chemisorption abilities and catalytic effects towards polysulfides have been incorporated with carbon matrices as sulfur hosts, separator modifications or cathode interlayers for Li-S battery. The research and development of iron-based nanomaterials towards Li-S battery generally focus on the following three aspects: First, modulating iron-based compound types to explore the catalytic and chemisorption properties of different iron compounds on polysulfides conversion such as iron oxides, iron carbides, iron nitrides, iron sulfides, iron-based heterostructures, Secondly, hybridizing iron-based nanomaterials with carbon substrates with different morphologies for increasing the conductivity of iron-based compounds and improving their catalytic features through various regulation strategies, including defect engineering, heterostructure construction, *etc.* Thirdly, regulating the adsorption abilities and catalytic effects for polysulfides conversion by adjusting the orbital energy level, energy band structure and charge distribution of iron-based nanomaterials.

Although iron-based nanomaterials have demonstrated outstanding electrochemical performances in Li-S battery, a comprehensive summarization about their application in Li-S battery and corresponding mechanist insights for the electrochemical performance enhancement has not been reported yet. Therefore, it is essential to give a timely review on the employment of iron-based nanomaterials in Li-S battery to clarify and highlight the origin

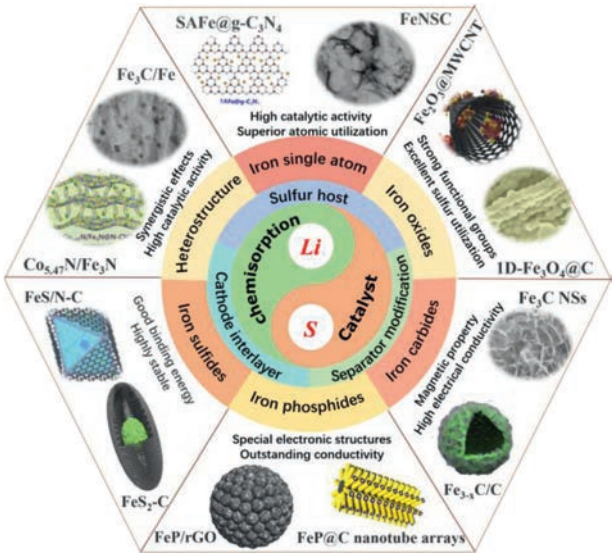

Fig. 2. Schematic illustration of the current publications on iron-based nanomaterials in Li-S battery according to material types and their advantages.

of internal activities. Fig. 2 summarizes the current publications on iron-based nanomaterials in Li-S battery according to material types. The introduction of iron-based nanomaterials into the highly complicated Li-S battery system can subsequently favor the effective entrapment for LiPSs, the LiPSs redox reaction kinetics acceleration and electronic conductivity enhancement, thus promoting the capacity and reversibility performances of Li-S battery.

In this review, for the first time, we systematically discuss the latest advances about popular iron-based nanomaterials applied in Li-S battery. On the basis of the recent progress, we elucidate the chemisorption and catalysis mechanisms of iron-based nanomaterials for the electrochemical reactions of Li-S battery comprehensively, and a perspective on their future research and development is also provided at last.

2. Fundamental understanding of iron-based nanomaterials by theoretical calculations

As a growing family of transitional metal compounds, iron-based nanomaterials have become one of the most suitable materials for grid-scale energy storage-conversion systems since their superior natural abundance, low cost, high safety and non-toxicity [31]. For Li-S battery, with the increasing studies of iron-based materials, researches have focused on the mechanistic insights into the chemisorption interaction and catalytic effects for polysulfides conversion theoretically. Density functional theory (DFT) calculation has been gradually applied to investigate their theoretic potential in performance improvement from an atomic level, providing an effective guideline to the rational design of iron-based chemical adsorbents and electrocatalysts.

In general, depending on synthesis methods, different types of iron nanomaterials (Fe_xO_y, Fe_xS_y, SA-Fe, Fe_xN_y, Fe_xC_y, Fe_xS_y, *etc.*) are obtained. The ionic bonds play a dominant role in the chemical interaction with polysulfides. For instance, Yang *et al.* [32] studied the adsorption mechanism of iron oxides towards polysulfides through the synthesis of three-dimensional (3D) hierarchical porous graphene macrostructure coupled with uniformly distributed αFe_2O_3 nano-particles (denoted as Fe-PGM) by implementing LiPSs static adsorption tests and DFT calculations, as shown in Fig. 3a(i). The αFe_2O_3 displayed a strong affinity towards LiPSs, which was mainly ascribed to the forceful bonding between Li (LiPSs)-O (αFe_2O_3) and Fe (αFe_2O_3)-S (LiPSs) ions according to the DFT calculation results (Fig. 3a(ii)). Moreover, with the sulfur chains shortening, the binding strength of Li-O and Fe-S both increased, correlated to the upward charge transferred from S-containing clusters to the substrate of αFe_2O_3. Consequently, iron oxides can restrain the shuttling of soluble polysulfides evidently *via* the powerful chemical interaction with LiPSs. Similar conclusions were promoted by Zhong *et al.* [33]. Combining X-ray photoelectron spectroscopy (XPS) results as shown in Fig. 3a(iii) and DFT calculations as we mentioned above, the authors found that the iron oxides can effectively immobilize LiPSs intermediates through the formation of Li-O and Fe-S bonds, while the Li-O bonds dominated in these two. On the other hand, XPS analysis was also utilized to confirm the bonding of Fe-S and Li-O as Fan *et al.* [34] and Li *et al.* [35] elucidated.

As with the iron oxides, iron sulfides also interact with polysulfides effectively through two atomic binding configurations from theoretical perspective in previous reports, namely S-binding and Li-binding (Figs. 3b(i) and (ii)), where the S-binding means Fe-S bond (S is from extrinsic adsorbates such as Li_2S), and Li-binding means Li-S bond where Li is from Li_2S. Chen *et al.* [36] demonstrated that for iron sulfides, S-binding was preferable to Li-binding. This was primarily concluded theoretically from the difference of the Mulliken charge change between the Li and S in Li_2S (denoted as Li_δ and S_δ, respectively, where δ refers to Li_2S). The Mulliken charge of S_δ changed from -1.780 to -0.630 after adsorbed by FeS, which was more obvious than that of Li_δ (from 0.890 to 1.030). Furthermore, it was revealed that the chemical S-binding formation is induced by electrons transferring form S_δ in absorbed Li_2S to Fe in FeS, of which the transferred electrons occupied the d-orbitals of Fe. Projected density of states (PDOS) analysis was also applied to reflect the obvious electron transfer between the 3d-orbitals of Fe and 3p-orbitals of S_δ as displayed in Fig. 3b(iii). Beyond that, another important surface property of iron sulfides was also judged according to the relative energy of lithium-ion diffusion barrier, which can influence the intercalation-deintercalation process of lithium and the reaction between lithium and sulfur significantly. As displayed in Fig. 3b(iv), there is a metastable point existing between two stable points in the bimodal curve of the lithium-ion diffusion pathway of iron sulfides, of which the relative energy (0.2 eV) is much lower than that of graphene materials (0.31 eV). The bonding configurations were further confirmed by Boyjoo *et al.* [37], which designed and fabricated the structure of highly dispersed pyrrhotite $Fe_{1-x}S$ nanoparticles embedded in hierarchically porous nitrogen-doped carbon spheres ($Fe_{1-x}S$-NC). To investigate the chemisorption capability theoretically, DFT simulations were conducted on various surface models with different d-orbital structures, including Fe_7S_8, FeS_2 and Fe_3S_4, which exhibited distinct adsorption energies for polysulfides theoretically and experimentally subsequently. In this work, Li_2S_8 was absorbed on iron sulfides through the bonding of both Li-S and S-Fe, while for other LiPSs, like Li_2S_2, Li_2S_4, Li_2S_6, showed the most stable adsorption structures with only Li oriented to the surface.

Beyond that, the electrocatalysts coupled with Fe-N active sites are the most studied iron-based compounds for accelerating polysulfides conversion, including single-atom (SA)-Fe and iron nitrides. The SA-Fe, usually incorporated in nitrogen-doped carbon (NG) matrix with plane-symmetric Fe-4 N coordination, whereas, the iron nitrides, for example, Fe_2N usually with triangular pyramidal Fe-3 N coordination (Fig. 4a(i)). According the DFT calculation results promoted by Ma *et al.* [38], the Li-N bonds and Fe-S bonds both emerged for their rationally synthesized SA-Fe/Fe_2N@NG (Fig. 4a(ii)), where N atoms were from the nitrogen-doped carbon and the Fe-S bonds were induced by the interaction between the Fe from SA-Fe (or Fe_2N) and the S from Li_2S. Interestingly, the SA-Fe and Fe_2N displayed different electronic distribution which can

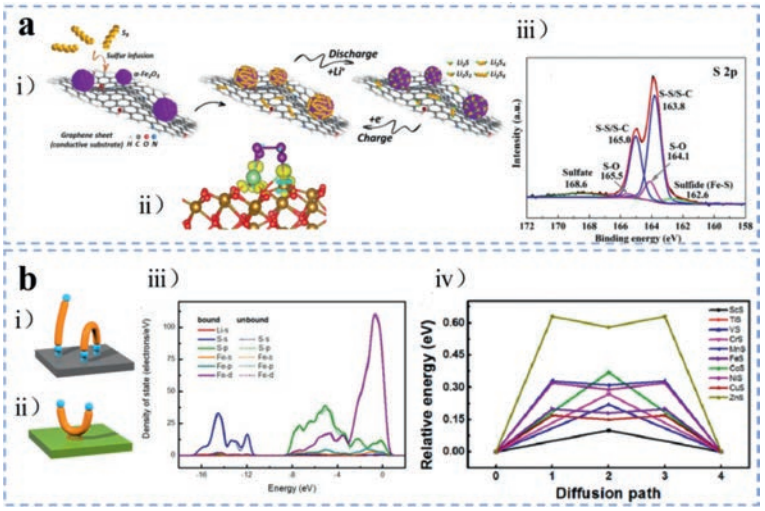

Fig. 3. (a) Fe-PGM: (i) Schematic of the conversion process of sulfur on the surface of Fe-PGM. (ii) Calculated differential charge density of the Li_2S_4 adsorption on αFe_2O_3. Green, purple, yellow, red and gray balls stand for the Li, S, Fe, O and C atoms, respectively. (iii) XPS curve of S 2p of Fe-PGM-S. Reproduced with permission [32]. Copyright 2017, Elsevier. (b) FeS: (i) Schematic illustration of Li-binding and (ii) S-binding. (iii) PDOS analysis of FeS. Solid line refers to iron sulfides bound with Li_2S, and dotted line, unbound with Li_2S. (iv) Energy profiles for diffusion processes of Li ion on various transition metal sulfides. Reproduced with permission [36]. Copyright 2017, American Chemical Society.

be attributed to their dissimilarity of coordination structure with N atoms. The SA-Fe allowed only one-site adsorption mechanism, while for Fe_2N, preferable to bind to the bridge site of two adjacent Fe sites on the surface as shown in Fig. 4a(iii). The synergistic effect of Fe and N dopants has been proved to be efficacious in boosting the anchoring ability of carbon materials towards polysulfides by Li *et al.* [39] and Zhang *et al.* [40]. What is more, Zeng *et al.* [41] elaborated how the Fe-N active sites improved the performance of Li-S battery by simulating the anchoring mechanism of single-atom Fe and N co-doped graphene with different number of N coordination (Fe_xN ($x = 1, 2, 3, 4$)). It was revealed that the chemisorption capability of polysulfides on Fe_xN was evidently enhanced than on pure graphene, which can be mainly credited to the strong orbital hybridization of Fe and S atoms, resulting in the formation of strong chemical Fe-S bonds. Li-N bonds were also demonstrated to be effective to contribute to improve the electrochemical performance and strengthen the stability of co-doped Fe_xN.

To further investigate the origin of catalytic activity of transitional metal based catalysts, Qian *et al.* [42] combined theoretical simulations with experimental measurements and unveiled that the d-band centers of metal atoms and the p-band centers of anions from metal compounds influenced their catalytic effects towards polysulfides reduction and oxidation significantly. The smaller energy band gap, the better polysulfides redox reaction reversibility. This theory provided a vital guidance in designing the iron-based catalysts. Yu *et al.* [43] fabricated carbon cloth with grown FeP@C nanotube arrays which exhibited a stronger affinity towards polysulfide species than that of Fe_3O_4 owing to the Li-P binding and Fe-S binding (Figs. 4b(i) and (ii)). It was notable that the superiority of chemisorption ability of FeP can be ascribed to the shift of the p band in FeP, which could accelerate the interfacial electronics transfer dynamics. The corresponding density of sates analysis as presented in Figs. 4b(iii) and (iv) revealed that the shift triggered a significant decrease of the energy gap between the energy centers of the Fe 3d and P 2p bands. Hence, the reduction of the energy gap between bonding and antibonding orbitals led to the P atoms more easily to combine with or detach from other atoms, bringing the promotion of electron transfer and LiPSs conversion dynamics. Other iron-based phosphide compounds were also explored *via* DFT calculations [44]. The chemical interactions were substantially originated from two configurations, the Li-P binding and Fe-S binding. The coexistence of these two binding endowed FeP material with remarkable capability to restrain LiPSs shuttle effect.

The polysulfide anchoring and converting activity of iron carbides were also investigated through DFT simulations. As elucidated by Zhou *et al.* [45], the structure of necklace-like Fe_3C/N-doped carbon nanoboxes (Fe_3C/NC) connected by N-doped carbon (NC) nanofibers was utilized as multifunctional sulfur hosts. The DFT calculations revealed that the N modified carbon formed Li-N bonds as displayed in Fig. 4c, while Fe_3C formed Li-C bonds and Fe-S bonds, respectively, enhancing the binding properties of polysulfide species effectively.

Concluding this section, theoretical studies based on DFT calculating or DOS analyzing underlined the origin of the superior adsorption capability and catalytic activity of iron-based compounds towards polysulfides. In general, the coexistence of two binding mechanisms as we mentioned above, which are Li-X binding (X represents heteroatoms such as O, N, P and S) and S-binding (S represents sulfur atoms from polysulfides), allows for powerful affinity through chemical interaction. Furthermore, a low lithium-ion diffusion barrier of polysulfides on the surface of iron-based compounds benefits the growth and deposition of insoluble Li_2S, leading to the promotion of polysulfide redox reaction kinetics. On the other hand, the electrochemical performance of Li-S battery system with iron-based nanomaterials as anchors or electrocatalysts was greatly enhanced due to their strong affinity and catalytic effects. The calculated theory about the energy centers of d/p bands elucidated to some extent why the electrochemical performance of different types of iron-based compounds varied.

3. Application of iron-based nanomaterials in Li-S batteries

3.1. Iron single-atom material

Single-atom composites (SACs), which consist of isolated metal atoms dispersed or anchored on matrices, have been regarded as rising stars in the field of catalysis recently [46]. With the merits of maximum atomic utilization, uniformly distributed active sites and splendid catalytic activity and selectivity, SACs have been widely employed in numerous electrochemical reactions, for instance, oxy-

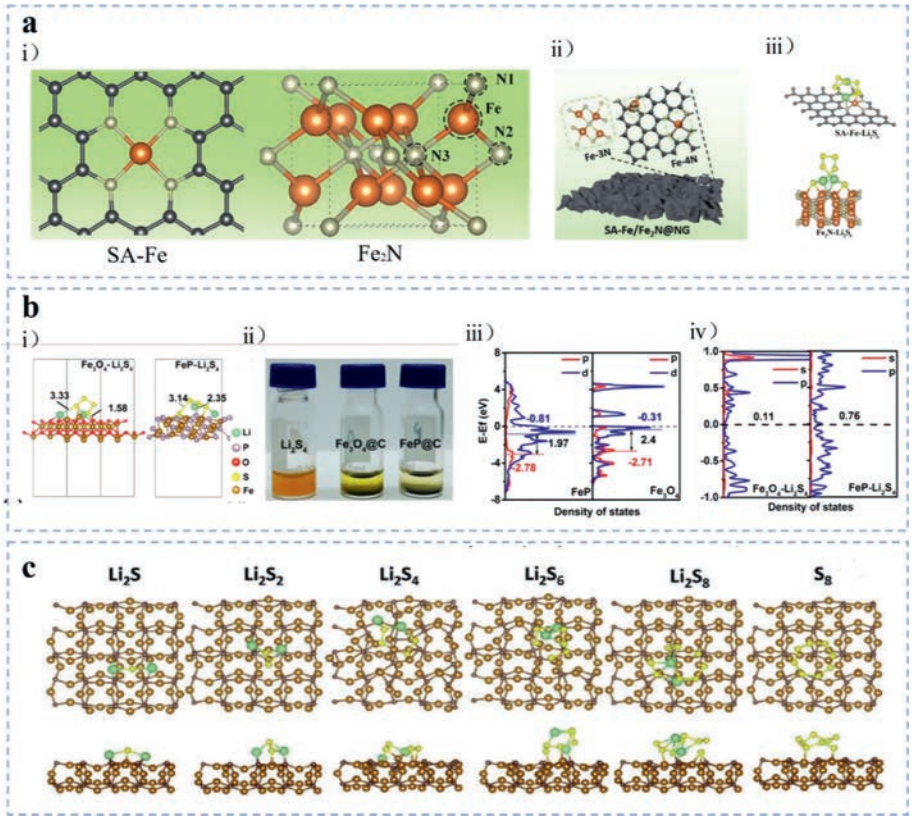

Fig. 4. (a) SA-Fe/Fe_2N@NG: (i) Simulated structural models of SA-Fe and Fe_2N. The black, gray, and orange balls refer to C, N and Fe, respectively. (ii) Schematic nanoarchitecture of SA-Fe/Fe_2N@NG. (iii) Optimized binding configurations of Li_2S_6 on SA-Fe and Fe_2N, respectively. Reproduced with permission [38]. Copyright 2021, Wiley-VCH GmbH. (b) FeP@C: (i) Simulated structural models of Fe_3O_4(111) and FeP(211) after Li_2S_4 absorption. (ii) Visual static adsorption tests of CF/Fe_3O_4 @C and CF/FeP@C with Li_2S_4. (iii) Density of states analysis (DOS) of p bands of anions and d bands of Fe in Fe_3O_4 and FeP. (iv) DOS of Li_2S_4 on Fe_3O_4(111)-Li_2S_4 and FeP(211). Reproduced with permission [43]. Copyright 2019, American Chemical Society. (c) Binding structures of LiPSs and S_8 on the Fe_3C(220) surfaces. Reproduced with permission [45]. Copyright 2021, Wiley-VCH GmbH.

gen reduction reactions [47], hydrogen evolution reactions [48] and advanced energy systems [49–51].

Among these, the latest researches revealed that the non-precious iron-based SACs, with stable and explicit active centers, can demonstrate the same or even better electrochemical performances than other traditional precious metal catalysts. In particular, iron-based SACs coordinated with nitrogen-doped carbon matrix have achieved much attention and great progresses as efficacious anchors and catalysts [52–54], especially in Li-S batteries [55–57]. For example, one of the early studies using iron-based SACs as sulfur hosts was reported by Liu and co-workers in 2018 [58]. The researchers fabricated the sulfur host material of single iron active sites in porous nitrogen-doped carbon (Fe-PNC, as shown in Fig. 5a(i)) through polymerizing and carbonizing diphenylamine in the presence of iron phthalocyanine and a hard template. With a sulfur loading of 1.3 mg/cm^2, the as-prepared Fe-PNC/S cathode displayed an initial specific capacity of 1138.6 mAh/g at 0.1 C and retained 427.1 mAh/g after 300 cycles (Fig. 5a(ii)). The morphology of Li_2S in both Fe-PNC/S and PNC/S after the first and second cycles at 0.1 C were also observed to clarify the comparison of phase nucleation overpotential for the formation of nanoscale Li_2S between Fe-PNC and PNC. It was notable that Li_2S nanospheres deposited on Fe-PNC/S cathode surface were smaller and held the morphology better in Fig. 5a(iii). Encouraged by the attractive surface chemistry of single iron atoms, Jiang *et al.* [59] developed novel self-supporting carbon nanofibers with hierarchical porous structure and Fe/N adsorption/nucleation centers (Fe/N-HPCNF) as high-performance sulfur hosts *via* a facile co-spinning method. Benefiting from the porous carbon fiber structure, electrolyte infiltration, conductivity, Li ion transportation rate and sulfur redox kinetics were all improved even with high sulfur loading. The evenly distributed Fe/N heteroatoms served as restraints on polysulfide diffusion through strong chemisorption and as regulators for homogeneous sulfur nucleation. Consequently, S@Fe/N-HPCNF cathodes presented a high initial specific capacity of 1273 mAh/g for over 500 cycles at 0.5 C (the sulfur areal density equals 3.5 mg/cm^2). There has been an increasing interest on utilizing iron-based SACs for Li-S battery systems as sulfur cathodes [60–63], separators [38,64,65] or cathode interlayers [66] to improve the polysulfide immobilization or sulfur species conversion. For instance, Wang *et al.* [60] fabricated a holey Fe, N co-doped graphene (HFeNG) *via* a one-step scalable calcination process. The corresponding sulfur cathodes delivered a high-rate capacity of 1154 mAh/g at 0.5 C initially and cycled stably with a slight capacity decay of 0.083% per cycle as displayed in Fig. 5b(ii). The electrochemical performance advancement can be attributed to the unique holey structures and the strong adsorption forces of Fe-N_2 at the edges which are represented in Fig. 5b(i). Considering the utilization efficiency of SACs, Zhang *et al.* [64] proposed a multifunctional commercial polypropylene separator coated by graphene foam impregnated with Fe SACs catalysts. As a result, the cycling stability improved hugely, with an initial specific capacity of 891.6 mAh/g and 83.7% retention after 750 cycles at 0.5 C.

Given the performance advancement arising from iron-based materials, many researches have been focused on the mechanist insights about the chemisorption capability enhancement and catalytic effect by theoretical analysis. Furthermore, Zhang *et al.* [67] investigated the anchoring mechanism of Fe-N_4/graphene to

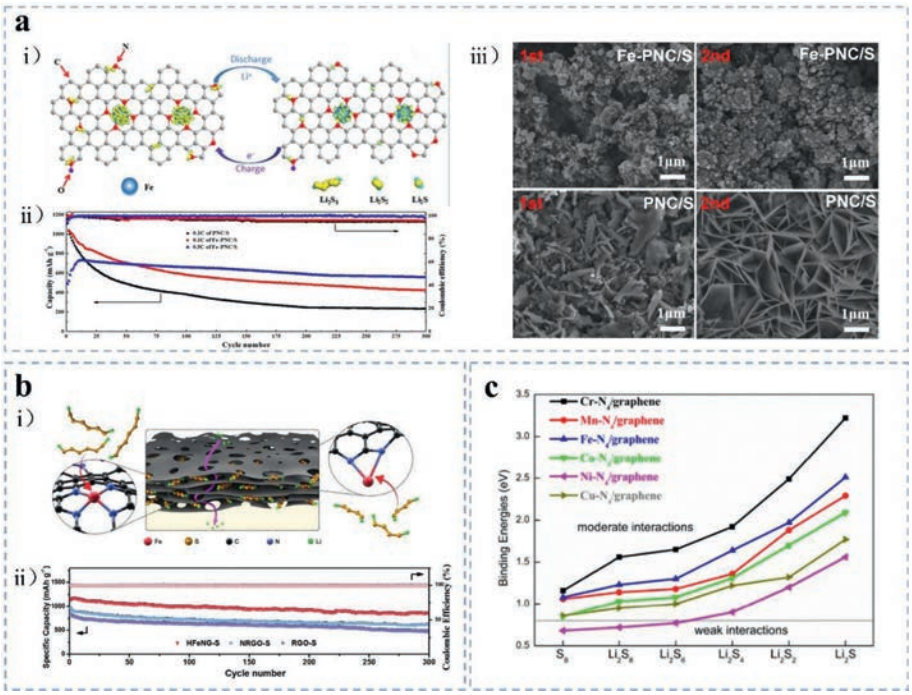

Fig. 5. (a) Fe-PNC: (i) Schematic diagram of the redox reaction of polysulfides catalyzed by single iron atoms on the surface of Fe-PNC. (ii) Long-term cycling stability of PNC/S and Fe-PNC/S electrodes at 0.1 C and 0.5 C, respectively. (iii) Micro morphologies of PNC/S and Fe-PNC/S electrodes after cycling at 0.1 C for the first and second cycle, respectively. Reproduced with permission [58]. Copyright 2018, American Chemical Society. (b) HFeNG: (i) Schematic elucidation of entrapment of sulfur species in the layered nanostructure and the additional lithium-ion diffusion pathways (purple arrow line) through the holey structure (the black sheets). (ii) The long cycling performance and relative Coulombic efficiency of RGO-S, NRGO-S, and HFeNG-S electrodes at 0.5 C. Reproduced with permission [60]. Copyright 2018, WILEY-VCH GmbH. (c) The computed binding energies of S-containing clusters on various metal-N_4/graphene. Reproduced with permission [67]. Copyright 2018, Elsevier.

LiPSs species by means of comprehensive DFT computations. The calculation results of binding energy suggested that the long-chain polysulfides can bind with Fe-N_4/graphene stably, with two interaction configurations of Fe-S bond and Li-N bond. The computed binding energies of S-containing clusters on various metal-N_4/graphene as shown in Fig. 5c revealed that Cr-, Mn-, Fe-, Co- and Cu-nitrogen/graphene exhibited optimal interaction with soluble lithium polysulfides due to the synergistic effects between the metal and N atoms, which not only effectively trapped the soluble lithium polysulfides to suppress the shuttle effect, but also well kept their cyclic structures. Notably, the Fe-N_4/graphene displayed an appropriate binding energy among them, which facilitates a smoother trapping-diffusion-conversion process of LiPSs [68,69]. The researchers also compared the electronic band structures of Co-N/graphene before and after polysulfides adsorption and found that there was a small band gap of less than 0.50 eV, which indicated the obvious intrinsic semiconducting nature of Co-N_4/graphene even after polysulfides adsorption. This theory also provides some experiences for Fe-N_4/graphene. However, the relationship between these two binding mechanisms still remained mysterious. Liang *et al.* [70] explored that there is a competitive relationship between Li-bonding and S-bonding. Moreover, the S-bonding configuration usually has better performance for both chemisorption and catalysis than Li-bonding. Similar results were obtained by Lin *et al.* [71] and Zhang *et al.* [40].

3.2. Iron oxides

Owing to the low cost, easy availability and strong functional groups on the surface, iron oxides, including FeO, Fe_2O_3, Fe_3O_4, *etc.* have been extensively applied in lithium-ion battery and sodium-ion battery since early stages [72–74]. However, the poor conductivity and uncontrollable size seriously retard the electrochemical performance of iron oxides. Hence, to overcome these limitations, hybridizing iron oxides with various carbon-based materials has been an effective way.

Iron oxides were used in lithium sulfur battery until 2017 by Yang *et al.* [32] as we mentioned above. Considering the large surface area and abundant pore structures which benefit sulfur utilization, iron-based metal-organic frameworks (MOFs) have been widely applied as precursors to synthesize iron oxides/carbon composite materials [34,75,76]. For example, Fan *et al.* [34] prepared a jujube pit like Fe_3O_4/C composite (Fe_3O_4/C) calcinated from Fe-MOFs (MIL-53), of which the schematic diagram is presented in Fig. 6a(i). After a facile melt diffusion technique, sulfur was loaded into the internal hollow space of Fe_3O_4/C. The static polysulfides adsorption tests and relative UV–vis adsorption spectrum proved the promotional adsorption capability of Fe_3O_4/C as shown in Fig. 6a(ii). Consequently, such Fe_3O_4/C/S cathodes displayed a high specific capacity of 819 mAh/g at 1 C, with 642 mAh/g retained after 300 cycles (Fig. 6a(iii)). Then Ding *et al.* [75] proposed an ordered microchannel graphene scaffold with incorporated catalytic MOF-derived Fe_3O_4 nanocrystals and porous carbon (denoted as Fe_3O_4/NC/G) as a multifunctional sulfur host, which exhibited a reversible specific capacity of 1007 mAh/g at 0.1 C, with a small capacity decay rate of less than 0.01% after 100 cycles as shown in Fig. 6b(i). Cyclic voltammetry tests of symmetric cells were performed to verify the catalytic effects of Fe_3O_4/NC/G towards polysulfide reaction kinetics and stability in Fig. 6b(ii). The higher current density and stronger redox peaks demonstrated that polar Fe_3O_4 nanocrystals accelerated the electrochemical reactions and expeditious conversion with catalytic effects. Furthermore, the conversion mechanism of Fe_3O_4/NC/G for Li-S battery was studied through *in-situ* X-Ray Diffraction (XRD) during cycling for the first 2 cycles at 0.1 C as elucidated in Fig. 6b(iii). During the discharge process, the signals of polysulfides intermediates almost disappeared, suggesting that the diffusion of long-chain LiPSs to the Li anode was greatly reduced and then the undesired anode

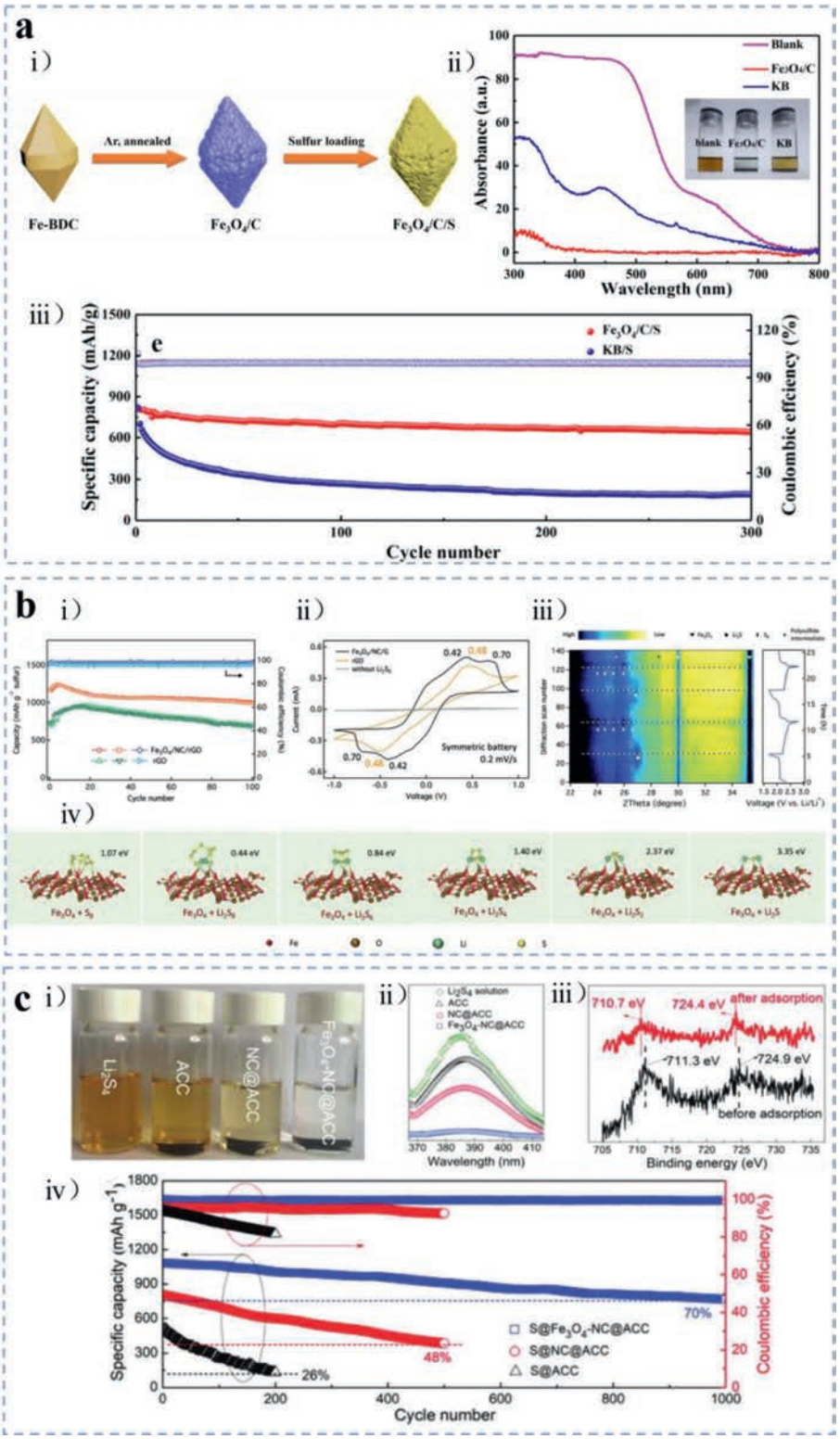

Fig. 6. (a) Fe_3O_4/C: (i) Schematic illustration of synthesis method of Fe_3O_4/C. (ii) UV–vis adsorption spectrum of the polysulfide solution after absorbed by Fe_3O_4/C and KB, and pristine polysulfide solution. (iii) Long-term cycling stability of KB/S and Fe_3O_4/C/S electrodes at 1 C. Reproduced with permission [34]. Copyright 2019, Elsevier. (b) Fe_3O_4/NC/G: (i) Cycling stability and relative coulombic efficiency of Fe_3O_4/NC/G and rGO aerogels with the Li_2S_6 catholyte at the current density of 0.1 C. (ii) CV curves of corresponding electrodes scanning at 0.2 mV/s. (iii) The cycling profiles of Li-S batteries with Fe_3O_4/NC/G/S cathodes within the first 2 cycles at 0.1 C and the correlative *in-situ* XRD patterns presented in a contour diagram. (iv) DFT simulated molecular nanostructures and adsorbent energies of sulfur and Li_2S_n on the surface of Fe_3O_4. Reproduced with permission [75]. Copyright 2019, The Royal Society of Chemistry. (c) Fe_3O_4-NC@ACC: (i) Visual polysulfides adsorption tests of ACC, NC@ACC, and Fe_3O_4-NC@ACC, with 5 mm Li_2S_4 solution immersed for 30 min. (ii) UV–vis adsorption spectra of corresponding solution after adsorption. (iii) XPS analysis of Fe 2p from Fe_3O_4-NC@ACC before and after polysulfides immobilization. (iv) Cyclic stability and Coulombic efficiency of corresponding electrodes as shown in the chart at 0.2 C. Reproduced with permission [77]. Copyright 2018, WILEY-VCH GmbH.

corrosion can be effectively suppressed. DFT calculations were also carried out to analyze the chemical interaction between Fe_3O_4 and polysulfides. The inferior bonding energy of Fe_3O_4 towards LiPSs (0.44–3.35 eV) was much higher than that of pristine carbon (0.10–0.52 eV), which can be credited to the strong polar-polar interaction between Fe_3O_4 and polysulfides. The accurate calculation results of binding energies of polysulfides on the surface of Fe_3O_4 were displayed in Fig. 6b(iv). Besides these Fe-MOFs derivatives, various iron oxide/carbon nanomaterials emerged through diverse synthesis methods. Lu *et al*. [77] reported a new approach to fabricate strongly coupled Fe_3O_4 and N-doped carbon which were grown on self-standing activated carbon fiber cloth, namely Fe_3O_4-NC@ACC. This unique nanostructure was obtained *via* pyrolysis of molecular mixtures of $Fe(CN)_6^{4-}$ and pyrrole which were coated on ACC. During the oxidation polymerization of pyrrole prompted by $Fe(CN)_6^{4-}$, the reduced $Fe(CN)_6^{4-}$ compounds would be incorporated in the PPy (polypyrrole) framework due to the chemical interaction between the C≡N ligands and pyrrole, which means, the Fe_3O_4 nanocrystals would be embedded in the carbon framework with rigid carbon layers covering the surface. In the LiPSs adsorption evaluation, the Li_2S_4 solution immersed with Fe_3O_4-NC@ACC exhibited nearly complete LiPSs adsorption within only 30 min as displayed in Fig. 6c(i), which can be ascribed to the chemical binding of strongly coupled Fe_3O_4 for LiPSs. The following UV–vis adsorption spectra and XPS analysis of Fe_3O_4-NC@ACC composite before and after LiPSs adsorption further proved that in Figs. 6c(ii) and (iii). Beyond that, the discharge capacity of S@Fe_3O_4-NC@ACC cathodes with varied crystallinity and Fe/N loading levels were analyzed in correlation with the reaction stages. By controlling the pyrolyzing temperatures and the amount of pyrrole, the discharge capacity occurred in stage III (from Li_2S_4 to Li_2S_2 and Li_2S) differentiated, suggesting the strongly coupled Fe_3O_4 and N-carbon played a key role in the improvement of short-chain polysulfide conversion. With these merits, as shown in Fig. 6c(iv) the S@Fe_3O_4-NC@ACC cathodes presented a high specific capacity of 1316 mAh/g at 0.1 C, and a retention of around 70% after 1000 cycles at 0.2 C under a high sulfur areal density of 4.7 mg/cm^2. Similar synthesis mechanism was utilized by Zhang *et al*. [78], but with different morphologies. Herein, novel hierarchical mesoporous nitrogen-rich carbon nanospheres comprising 1D carbon nanotubes encapsulating Fe_3O_4 nanoparticles (Fe_3O_4@CNTs nanospheres) were manufactured as sulfur hosts. Supported by the theoretical simulations, the soluble polysulfides interacts with iron oxides stronger than with carbonaceous material, thus alleviating the shuttling effect of LiPSs effectively. Benefiting from the synergistic effect of chemical adsorption and redox reaction catalyzing, the S/Fe_3O_4@CNTs cathodes displayed the specific discharge capacity change from 937.6 mAh/g initially to 538.5 mAh/g after 1800 cycles at 1 C. Iron oxides can also be obtained through the pyrolysis of iron oleate according to He *et al.*s' report [79]. The researchers assembled core-shell structured Fe_3O_4@C nanodots with 5 nm diameter as a valid sulfur host, of which the specific surface area reached 216.2 m^2/g owing to the nanosized structures of Fe_3O_4 particles. Due to the porous structures and loose surface of Fe_3O_4@C, the sulfur content of S/Fe_3O_4@C host material was calculated to be 66%. And the resultant S/Fe_3O_4@C cathode showed a high initial capacity of 1089 mAh/g at 0.2 C and 816 mAh/g at 1 C.

3.3. Iron carbides

Iron carbides have attracted intensive attention because of their potential utilization in the field of catalysis and energy storage systems, which can be obtained through versatile synthesis methods, such as sol-gel method, high temperature organic phase method, physical vapor deposition [80]. Notably, the unique electronic, catalytic and magnetic properties of iron carbides originated from their intrinsic structures favor their usage in Li-S batteries [81–83].

For instance, inspired by the work of introducing ferroelectric $BaTiO_3$ (BTO) into the sulfur cathode to control the "shuttle effect" of polysulfides by the "spontaneous polarization" of BTO [84], Gao *et al*. [85] introduced ferromagnetic iron/iron carbide (Fe/Fe_3C) nanoparticles with a graphene shell (Fe/Fe_3C/graphene) onto a flexible activated cotton textile (ACT) fiber to prepare the ACT@Fe/Fe_3C/graphene sulfur host. The innovation spot was that the path of the dissolved negative polysulfide ions can be altered *via* Lorenz force since the built-in magnetic field brought by ferromagnetic iron carbides, namely the "shielding effect" *via* ferromagnetic nanoparticles. In order to study the polysulfide trapping mechanism of magnetic Fe/Fe_3C nanoparticles, custom-design liquid cells of ACT@Fe/Fe_3C/S were performed in comparison with that of ACT/S. The strikingly different polysulfide diffusion behavior shown in Figs. 7a(i) and (ii) unveiled that the magnetic field can alter the diffusion path of LiPSs effectively through Lorenz force. In the following schematic illustration of Fig. 7a(iii), it can be found that owing to the instinctive magnetization of Fe/Fe_3C NPs, the generated magnetic field manipulated the motion of polysulfide ions through attracting them to the cathode side, thus resulting in a darker brown region of electrolyte around. Wei *et al*. [86] fabricated ordered mesoporous graphitic carbon/iron carbide nanocomposites (GC/Fe_3C) as sulfur host materials *via* an evaporation-induced self-assembly (EISA) procedure combined with Teflon-assisted solid-state decomposition. Herein, the Fe_3C nanocrystals contributed to catalyzing the graphitization of amorphous carbon, increasing its pore size. The large quantity of micropores and small-size mesopores enabled the hybrid framework a large specific surface area of 3105 m^2/g and pore volume of 3.32 cm^3/g, which guaranteed a high sulfur loading (85%) and alleviated the volume expansion to some extent. The as-prepared cathode displayed excellent capacity and cycling stability, with an initial discharge capacity of 1203 mAh/g at 0.2 C and a retention of 91.4% after 500 cycles. Wang *et al*. [87] also designed and synthesized a unique porous and conductive nanocomposite for which Fe_3C nanoparticles are embedded in nitrogen-doped porous carbon sheets (Fe_3C@NPCS). The porous carbonaceous nanostructures can provide more accommodation space for sulfur species and Fe_3C nanoparticles can enhance the electronic conductivity of the composite (Fig. 7b(i)). According to DFT simulations presented in Fig. 7b(ii), Fe_3C exhibited strong affinity towards polysulfides through Fe-S bonds. Benefiting from the outstanding conductivity of Fe_3C nanocrystals, the Fe_3C@NPCS-S cathode showed a reduced polarization and enhanced reversibility compared with NPCS-S in cyclic voltammogram (CV) measurements as demonstrated in Fig. 7b(iii). More importantly, as exhibited in Fig. 7b(iv), the Fe_3C@NPCS-S electrodes delivered greatly improved specific discharge capacities of 1251, 1127, 1020, 907, 802, 731 and 647 mAh/g at 0.2 C, 0.3 C, 0.5 C, 1 C, 2 C, 3 C and 5 C, respectively. The well-performed rate capability further proved that the introduction of Fe_3C nanocrystals facilitated the electrochemical kinetics, internal resistance and charge transfer as previous research reported. Apart from the increasing utilizations in sulfur hosts [88–91], iron carbides have also represented their advantages of superior conductivity in the application of interlayers for separators [92,93] or electrodes [94–96]. For example, as Song *et al*. [92] proposed, the MOF-derived Fe_3C nanocrystals compounded with the nitrogen-doped graphene-like carbon nanosheet (Fe_3C/NG) were coated onto separators given the catalytic and conductive properties of Fe_3C. The Li-S cell with a lightweight Fe_3C/NG-coated separator demonstrated splendid rate performances and cycling stability. Specifically, the as-prepared cell delivered an initial discharge specific capacity of 954.5 mAh/g even at a high current density of 6 C and maintained 439.9 mAh/g after 500 stable cycles with a sulfur loading of 1 mg/cm^2.

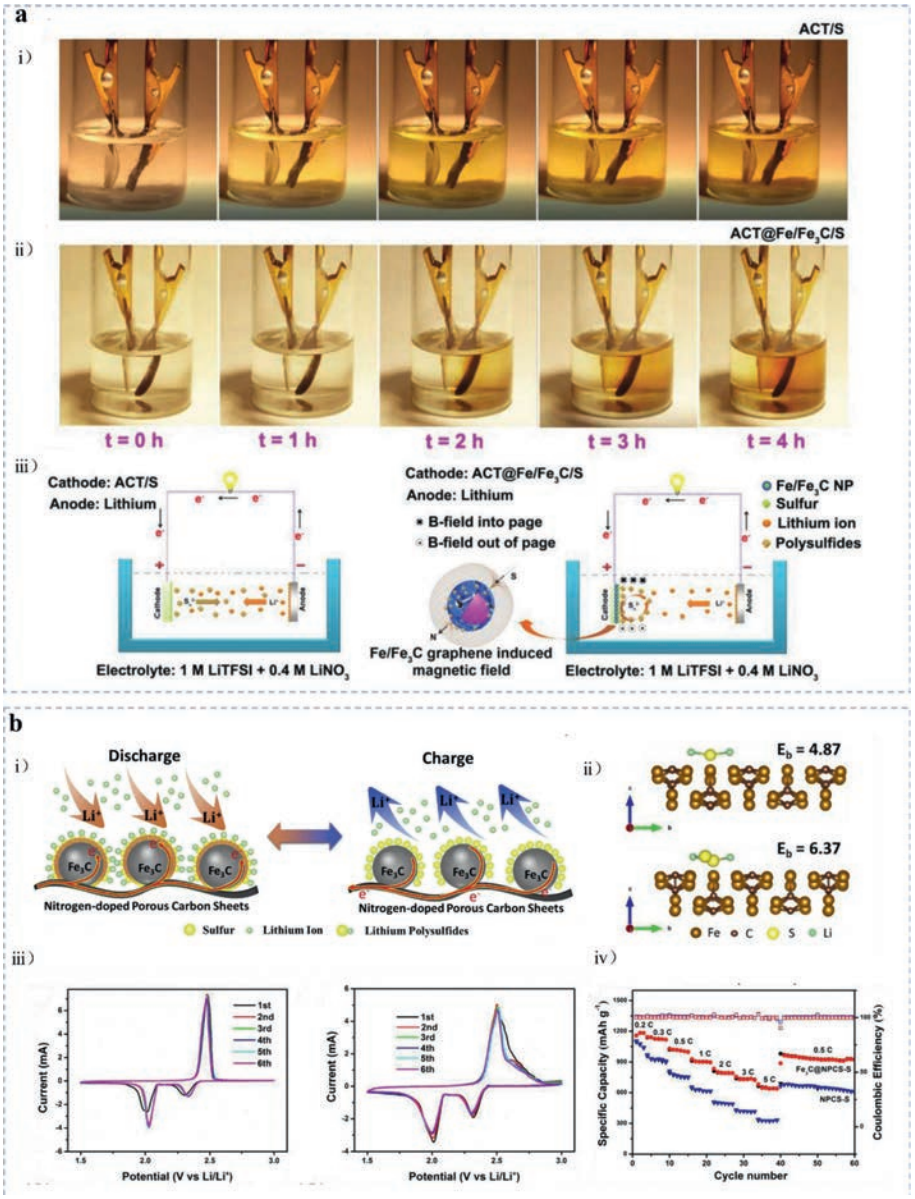

Fig. 7. (a) ACT@Fe/Fe_3C/S: Digital images of (i) ACT/S and (ii) ACT@Fe/Fe_3C/S electrodes during the first cycle in a liquid cell under a current density of 0.1 mA/cm^2. (iii) Schematic illustration of the polysulfide entrapment mechanism through Fe/Fe_3C NPs in the ACT@Fe/Fe_3C/S cathode. Reproduced with permission [85]. Copyright 2018, WILEY-VCH GmbH. (b) Fe_3C@NPCS: (i) Schematic diagram of the influence of as-proposed Fe_3C@NPCS in Li-S battery system, with porous nanostructures accommodating more sulfur and polysulfides, enhanced conductivity supported by Fe_3C NPs. (ii) DFT calculated binding energy (E_b) of Li_2S and Li_2S_2, respectively on the Fe_3C(100) surface. (iii) CV curves of Fe_3C@NPCS-S electrodes (right) and NPCS-S electrodes (left) at a scan rate of 0.1 mV/s. (iv) Rate performance with relative Coulombic efficiency of Fe_3C@NPCS-S and NPCS-S electrodes at different current densities from 0.2 C to 5 C. Reproduced with permission [87]. Copyright 2018, Elsevier.

Zhang *et al.* [94] fabricated freestanding graphitized carbon interlayers decorated with Fe/Fe_3C nano-catalysts acquired by thermal treatment of cellulose paper with adsorbed ferric nitrate at 1000 degrees. The *in-situ* grown Fe nanoparticles can promote the graphitization of carbon, enhancing the conductivity of interlayers. Thanks to the rationally designed nanoarchitecture and the efficacious acceleration of Fe/Fe_3C nanocrystals towards polysulfide conversion, the Li-S cell with an optimal carbon/Fe/Fe_3C interlayer displayed an initial specific capacity of 1556 mAh/g at 0.1 C and stabled at around 772 mAh/g at 1 C after 200 cycles.

3.4. Iron phosphides

Originated from the multi-electron orbitals of phosphorus, the superior chemical properties of iron phosphides have prompted their thriving development in catalytic applications in hydrogen evolution reaction (HER), and oxygen reduction reaction (ORR), lithium-ion batteries (LIBs), sodium-ion batteries (SIBs) and supercapacitors [97,98]. As reported in ORR catalysis, the lone pair electrons in the 3p orbital of phosphorus can result in a correlated local concentrated charge density, and the empty 3d orbital can supply with accommodation for the lone pair electrons from the p orbital of oxygen molecule, thus promoting the activity of phosphide catalysts [99], besides, the low cost, high conductivity and special electronic structures boost the application of iron phosphides in catalysis and energy storage systems.

Until recently, iron phosphides have demonstrated their superiorities in Li-S batteries [100–104]. Chen *et al.* [105] manufactured a phosphorized rGO/CNTs hybrid aerogel with embedded FeP nanocubes (p-HA/FeP) through the instant freezing and phosphorization of Fe-MOF precursors as shown in Fig. 8a(i). With the strong affinity of FeP NPs towards polysulfide immobilization, and

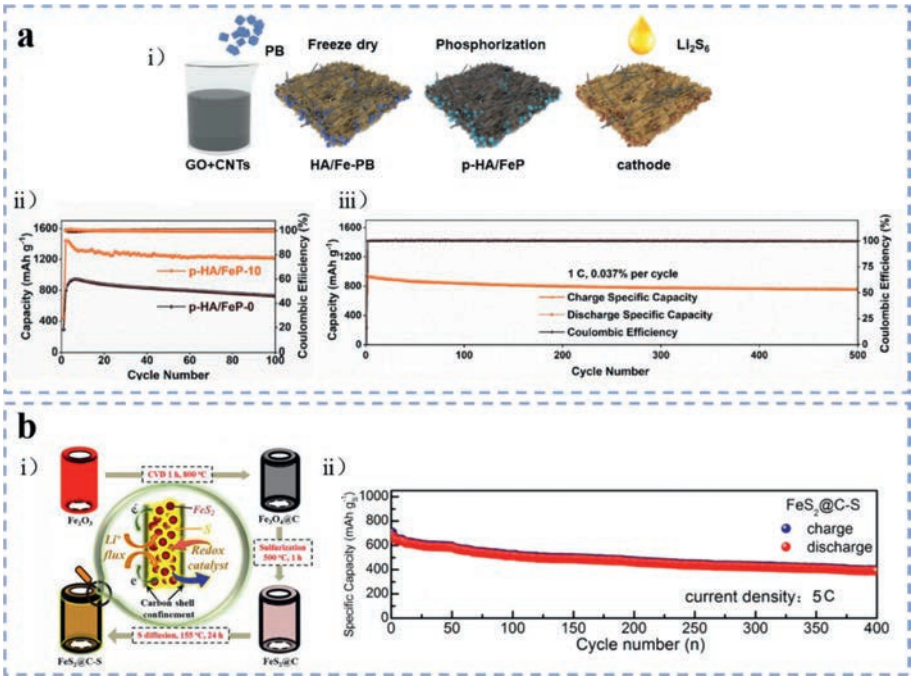

Fig. 8. (a) p-HA/FeP (phosphorized GO/CNTs hybrid aerogel embedding FeP nanoparticles): (i) Schematic illustration of synthesis process of the p-HA/FeP/S cathode. (ii) Cycling performance and Coulombic efficiency of p-HA/FeP/S electrode at 0.2 C. (iii) Long-term cycling stability with relative Coulombic efficiency of p-HA/FeP/S electrode at 1 C. Reproduced with permission [105]. Copyright 2020, Elsevier. (b) FeS_2@C: (i) Schemed synthesis process of FeS_2@C composite as well as the promotion mechanism of Li ions transportation and sulfur species redox reactions. (ii) Prolonged cycling stability of FeS_2@C-S cathode at a high current density of 5 C. Reproduced with permission [111]. Copyright 2020, American Chemical Society.

the sufficient interfaces for charge transformation offered by the conductive and microporous carbon scaffold, as well as the potential catalytic effects of FeP NPs for accelerating polysulfide redox reaction, the corresponding p-HA/FeP/S cathode delivered a high specific capacity of 1312.3 mAh/g at 0.2 C and maintained a lifespan of over 500 cycle at 1 C with only 0.037% capacity decay rate per cycle (Figs. 8a(ii) and (iii)). Li *et al.* [106] reported a facile approach to synthesize hierarchically structured composite of Fe_2P@nitrogen, phosphorus co-doped carbon (Fe_2P@NPC). Herein, Fe_2P nanoparticles were produced *via* the direct biological recycling of iron metal from electroplating sludge using bacteria, resulting in the uniform distribution of nanosized Fe_2P. According to DFT calculations, Fe_2P can not only suppress the polysulfide shuttling effect through strong chemical adhesion ability, but also facilitate the decomposition of insoluble Li_2S during the delithiation process. Meanwhile, with the merits of the multiple channels for ions transportation and adequate space for volume expansion, the Fe_2P@NPC/S cathode exhibited an obviously improved initial specific capacity of 1555.7 mAh/g at 0.1 C and prolonged cycling for 500 cycles with a reversible specific capacity of 761.9 mAh/g at 1 C.

3.5. Iron sulfides

Considering that the d orbital electron layer of the metal cation in transitional metal sulfides is more easily to obtain or lose electrons, which facilitates their utilizations in electrochemical catalysis, iron sulfides have been expected as cost-efficient and efficient alternatives for noble Pt-based catalysts. Additionally, iron sulfides usually possess high conductivity and appropriate chemical bond intensity for catalyzing conversion reactions [68,107]. However, the irresistible volume change during cycling and difficult synthesis methods hinders the practical applications of iron sulfides. Hence, in the field of Li-S battery, an increasing number of efforts have been devoted to explore and develop iron sulfides with different morphologies and hybridized matrices to overcome these obstacles [108–110].

After systematical investigation of the immobilization effects and mechanisms of transitional metal sulfides (Fe, Co, Ni, Cu, Zn, *etc.*) by Chen *et al.* [36], diverse iron sulfides have been dedicated to sulfur cathodes. For instance, Zeng *et al.* [111] fabricated sulfur cathode composites with FeS_2 nanoparticles encapsulated in hollow carbon shells through a facile way (Fig. 8b(i)). In addition to the enhanced adsorption capability towards polysulfides arising from FeS_2 which was confirmed by FTIR, Raman, and XPS analysis, more importantly, FeS_2 also demonstrated remarkable electrocatalytic effects in Li-S battery. In the CV measurements of FeS_2@C-S and MC/S cathodes, the cathodic and anodic peaks of FeS_2@C-S cathode were sharper than those of MC/S cathodes (mesoporous carbon/S), as well as the higher current densities, suggesting the improved redox reaction kinetics attributed to FeS_2. The FeS_2@C-S electrode exhibited a reversible specific discharge capacity of 800 mAh/g after cycling for 200 rounds at 0.2 C, while for the MC/S electrode, the specific discharge capacity faded to 200 mAh/g after only 50 cycles at 0.2 C. Even at a current density of 5 C, the FeS_2@C-S electrode still delivered a reversible discharge specific capacity of ~400 mAh/g after cycling for 400 times as shown in Fig. 8b(ii). Similarly, Li *et al.* [112] reported a rationally designed nanoarchitecture of N-doped carbon-coated iron sulfide (abbreviated as FeS/N-C) as sulfur hosting material fabricated through a simple pyrolysis method. With the virtues of abundant sulfiphilic sites for immobilizing polysulfides and catalyzing polysulfide conversion, the FeS/N-C based sulfur cathode showed a significant cycling stability promotion, with a stable discharge specific capacity of ~729 mAh/g retained after 500 cycles at 0.5 C.

3.6. Others

In addition to the simple inorganic compounds, there have been increasing attention in other binary inorganic or organic iron-based

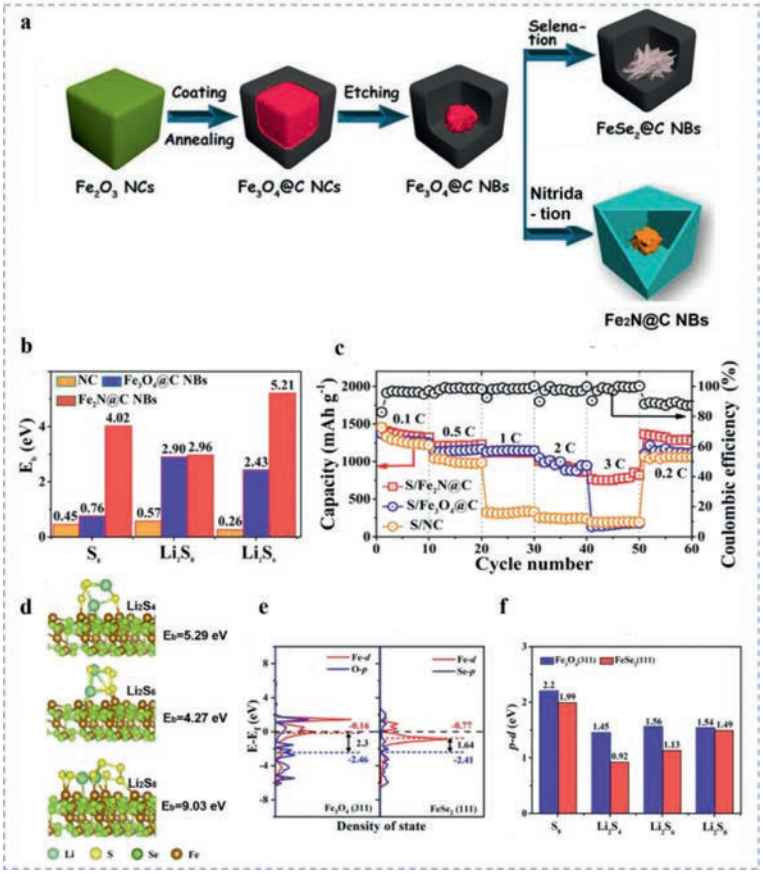

Fig. 9. (a) Schematic illustration of the fabrication process of Fe_2N@C NBs and $FeSe_2$@C NBs. (b) DFT calculated binding energy of relative sulfur species on NC, Fe_3O_4 and Fe_2N. (c) Rate performance of corresponding electrodes at current densities from 0.1 C to 3 C. (d) DFT calculated binding energy of Li_2S_n ($n = 4$, 6, 8) on the $FeSe_2$(111) surface. (e) DOS patterns of p bands of anions and d bands of Fe in the correlative Fe_3O_4(311) and $FeSe_2$(111). (f) Calculated energy gap values of $FeSe_2$ and Fe_3O_4 after absorbed by S_8, Li_2S_4, Li_2S_6, and Li_2S_8. (a-c) Reproduced with permission [121]. Copyright 2019, American Chemical Society. (a, d-f) Reproduced with permission [123]. Copyright 2021, Elsevier.

compounds or heterostructures for ameliorating the electrochemical performance of Li-S battery, such as iron-based MOFs [113–115], multi-metallic alloy [116–119] and other iron-based compounds or heterostructures [120].

Taken the marvelous porosity and crystallinity of pristine MOFs in account, most studies in the past decades focused on the modification of MOFs derivatives due to the poor conductivity of MOFs, however, the application of pristine MOFs as cathode materials in Li-S battery attracts researchers' attention until currently. For example, Benítez group [113] synthesized MIL-88A based on iron fumarate, which possessed a central prismatic portion and pyramidal terminal portions, resulting in a dual micro-mesoporous MOF system. The relative MIL-88A@S composite cathode displayed an initial discharge specific capacity of around 400 mAh/g at 0.1 C. Meanwhile, iron-based multi-metallic alloys exhibited great potential as catalysts for Li-S battery since their simpler and more suitable synthesis methods for practical utilizations. According to Chen *et al.*s' report [116], during the thermal treatment at a high temperature, Fe^{3+} and Ni^{2+} can be transformed into $FeNi_3$ as well as catalyze the graphitization of carbon materials, thus upgrading the electronic conductivity of carbon-based sulfur hosting materials. Confirmed by DFT calculations and experimental results, the bimetallic alloy $FeNi_3$ played a vital role in impeding polysulfide shutting effect through its chemical adsorption ability and catalyzing polysulfide conversion reaction.

Recently, in the case of metal catalysts, transition-metal-based alloys or intermetals have gained promising applications in catalyzing gas involved electrochemistry due to their high activity and stability arising from their good electronic and chemical properties. Considering the similar chemical property of oxygen and sulfur, researchers explored the functional mechanism of intermetallic catalysts in Li-S electrochemistry. For example, Manthiram group [117] reported a cost effective hexagonal close-packed (hcp)-phase Fe-Ni alloy serve as an efficient electrocatalyst to promote the LiPS conversion reaction in Li-S batteries. The electrocatalysis mechanisms of Fe-Ni toward LiPS conversion is considered that both the pristine nanosized Fe-Ni phase and the thin layer coated on the Fe-Ni alloy consists of various sulfurized phases provide high catalytic activity, thus the Fe-Ni alloy delivers a long lifespan over 800 cycles and high areal capacity of 6.1 mAh/cm^2 under lean electrolyte conditions with high sulfur loading of 6.4 mg/cm^2. Yang *et al.* [118] reported Ni_3Fe as electrocatalyst to enhance efficient polysulfide-involving surface reactions. They claimed the incorporation of iron into nickel phase induce strong electronic interaction and lattice distortion and promotes the redox kinetics of the multiphase conversion in Li-S electrochemistry. The 70 wt% sulfur cathodes with Ni_3Fe-modified separator delivers initial capacities of 1310.3 mAh/g at 0.1 C and 598 mAh/g at 4 C as well as stable long cycle life of 1000 cycles with low-capacity fading rate of ~0.034% per cycle.

Considering the benefits of iron-based compounds, our group has explored the promotion effects of iron nitrides [121] towards Li-S battery system. The yolk-shelled Fe_2N@C nanoboxes were designed and fabricated through hard-templating method using Fe_2O_3 as precursor and etching core for the conversion into Fe_2N (Fig. 9a). The as-prepared yolk-shelled Fe_2N@C nanoboxes can

provide strong chemical affinities, efficacious catalytic effects and electronic conductivity arising from polar Fe_2N cores, and sufficient loading space for sulfur due to the large internal void. With the support of Fe_2N cores, the binding energy of LiPSs on the surface of the as-proposed cathode composites were further confirmed to be greatly advanced through DFT calculations as shown in Fig. 9b. And the advancement can be attributed to the chemical Fe-S and Li-N binding configurations. In the relative rate performance as shown in Fig. 9c, the S/Fe_2N@C NBs and S/Fe_3O_4@C NBs electrodes delivered similar electrochemical performance from 0.1 C to 2 C, however, when the current density raised to 3 C, the S/Fe_2N@C NBs electrode still exhibited a specific capacity of 778 mAh/g while the S/Fe_3O_4@C NBs electrode reached only 161 mAh/g, demonstrating the superior rate capability of S/Fe_2N@C NBs electrode under higher current densities, which can be ascribed to the faster charge transfer dynamics and accelerated redox kinetics prompted by Fe_2N dominantly.

Benefiting from the considerable electrical conductivity, vigorous catalytic effect and cost effectiveness, iron-based chalcogenide compounds including iron-sulfides, iron-selenides have been widely employed in Li-S battery and displayed extraordinary electrochemical performance. Notably, iron-based selenides have displayed their advantages in ORR [122], which enlightens their potential utilizations for high-performance Li-S batteries since the similar redox mechanism between oxygen and sulfur electrochemistry. In this work, our group encapsulated $FeSe_2$ nanoparticles inside the hollow carbon nanocubes, promoting the electrochemical performance of Li-S cell through strong polysulfide immobilization and catalytic effect [123]. The binding energy of Li_2S_n ($n = 4$, 6, 8) on the $FeSe_2$(111) surface were simulated through DFT calculations as shown in Fig. 9d, which ranged from 4.27 eV to 9.03 eV, much higher than those on Fe_3O_4(311) surface. Furthermore, in the long-term cycling stability test, the S/$FeSe_2$@C electrode still retained 684 mAh/g discharge specific capacity at 1 C after 700 cycles, with an ultralow decay rate of 0.04% per cycle. In order to investigate the nature of the remarkable enhancement of electrochemical performance triggered by $FeSe_2$ NBs, DOS analysis of pristine $FeSe_2$ and Fe_3O_4 were performed in comparison as shown in Fig. 9e. Combined with the corresponding calculated energy gap of $FeSe_2$ and Fe_3O_4 after absorbed by S_8, Li_2S_4, Li_2S_6, and Li_2S_8, respectively (Fig. 9f), the patterns revealed that the energy gap values of original $FeSe_2$ and $FeSe_2$ after adsorbed polysulfides were all smaller than those of Fe_3O_4, which enable Se ions more easily to interact with polysulfides.

To achieve multiple functions of individual component, heterostructured materials attracted increasing attention due to their extraordinary strengths towards effective adsorption and catalytic conversion of LiPSs. The rational design and construction of multiple solid-state materials into heterostructures which take advantageous synergistic effects provide a common strategy to address the longstanding intrinsic issues of Li-S batteries. Lee *et al.* [124] fabricated conductive $Co_{5.47}N/Fe_3N$ heterostructures wrapped with 3D nitrogen-doped CNTs and graphene framework (3D $Co_{5.47}N/Fe_3N$@N-CNT-G) to improve the electron and lithium-ion transport. The synergistic effect of high electrocatalytic activity of polar $Co_{5.47}N/Fe_3N$ heterostructure can provide strong LiPS adsorption, accelerate the LiPS conversion reaction, control the kinetic behaviors of dissolved LiPS, and promote the Li_2S nucleation. The sulfur loaded 3D $Co_{5.47}N/Fe_3N$@N-CNT-G/S cathode delivered a capacity of ~1293 mAh/g at 0.1 C and a low degradation capacity of 0.019% per cycle for 500 cycles at 1 C rate.

4. Summary and future perspectives

In general, in order to promote the electrochemical performance of Li-S battery through trapping soluble polysulfide shuttling effect and boosting the electrochemical kinetics, it has been proven to be an effective strategy to induce transitional-metal compounds as chemical anchors and electrocatalysts. Among the various transitional metals, iron has exhibited superiority in Li-S battery owing to its low cost, environmental friendliness, similar characteristics of rich raw materials and high catalytic activity.

In this review, we concluded the paramount findings and the recent progress in iron-based nanomaterials for rechargeable Li-S battery. We summarized the mechanist insights towards the anchoring and catalytic effect of diverse iron-based nanomaterials for polysulfides entrapment and conversion. Through the discussion on the electrochemical performance of different iron-based materials, including iron single-atom material, iron oxides, iron carbides, iron phosphides, iron sulfides, iron-based heterostructure and so on, the intrinsic natures of various iron-based nanomaterials for realizing high performance Li-S battery have been elucidated. Table 1 condenses the electrochemical performance of some typical recently proposed iron-based nanomaterials which were utilized in Li-S battery system.

With the aim of advancing electrochemical performance and practical utilization of Li-S battery, balancing the polysulfides trapping and diffusive capability as well as conductivity of cathodes appears to be predominant. Overall, several predominant concerns and opportunities in future development are proposed as follows:

(1) Optimizing nanostructures with enhanced electrical conductivity and mechanical flexibility, such as 2D ultrathin materials and 3D hierarchical porous materials, are pivotal to the sufficient utilization of sulfur active species. Faster electron transportation can diminish the overpotential at the cathode interface. Other than introducing different carbonaceous substrates into cathodes, interface engineering on the electrode surface or separators has also been applied as an effective method to modify the conductivity or mechanical flexibility of battery system. On the other hand, to obtain higher energy density of electrodes, the sulfur loading should be as further improved with abundant accommodation space of rationally designed nanostructures.
(2) Engineering the structures and compound elements of iron-based nanomaterials as chemical anchors and electrocatalysts in Li-S battery enables superior specific capacity and excellent rate performance, which can be credited to the special electric structures of iron-based nanomaterials. However, the type and the content of multifunctional iron-based materials influences the electrochemical performance of batteries obviously, which is mainly due to the diverse electron structures, resulting in different chemical immobilization ability and catalytic effect. Therefore, the iron-based electrocatalysts should be well-characterized using XRD, SEM, TEM, XPS, and XAS and other measurements during the interval of Li-S measurement, to monitor the local structure and the variation of composition.
(3) Although the application of iron-based nanomaterials in Li-S battery is in its preliminary stage of exploration, there are still substantial space for further development. Apart from modulating the morphology, composition, and surface electronic structure of iron-based nanomaterials for Li-S battery, more essentially, clearer fundamental understanding of the chemical entrapment and catalytic mechanism towards polysulfides from an atomic level is required. Until now, the real active site and the detailed catalytic mechanism of iron-based catalysts are still lack of in-depth research. A deep understanding of the catalytic mechanism and the precise role of iron is important to clarify design guideline for the high-efficiency electrocatalysts in Li-S chemistry. More *in-situ* techniques should be developed to monitor the intermediates and the conversion process of sulfur species in Li-S batteries.

Table 1
Summary of electrochemical performance parameters for multifunctional iron-based nanomaterials in Li-S battery system.

Iron-based nanomaterial		Initial capacity (mAh/g)	Reversible capacity (mAh/g)	Rate (C)[a]	Lifespan	Capacity decay rate per cycle (%)	E/S ratio (μL/mg)[b]	Sulfur loading (mg/cm^2)	Ref.
Iron single-atom material	Fe-PNC/S	1138.6	427.1	0.1	300	0.2	N/A	1.3	[58]
	S@Fe/N-HPCNF	1273	857	0.5	500	0.06	8.5	3.5	[59]
	HFeNG–S	1154	866.6	0.5	300	0.083	10	2,3,5	[60]
Iron oxides	Fe_3O_4/C/S	819	642	1	300	0.07	N/A	1	[34]
	Fe_3O_4/NC/G	1017[c]	1007	0.1	100	~0.01	15	3.85	[75]
	S@Fe_3O_4-NC@ACC	1114	780	0.2	1000	0.03	N/A	4.7	[77]
Iron carbides	GC/Fe_3C	1203	1100	0.2	500	0.01	50	2	[86]
	Fe_3C@NPCS-S	1150	676	0.5	300	0.135	N/A	1.5	[87]
	Fe_3C/NG-coated separator	1248	1020.6	0.5	300	0.06	N/A	1	[92]
Iron phosphides	FeP/S	820.2	628.2	1	200	0.11	N/A	1	[102]
	Fe_2P@ NPC/S	865.7	761.9	1	500	0.04	12	2.6	[106]
Iron sulfides	FeS_2@C-S	N/A	800	0.2	200	N/A	N/A	1.5	[111]
			400	5	400				
	FeS/N-C/S	779.6	729.0	0.5	500	0.013	N/A	1.5	[112]
Others	MIL-88A@S	~400	~200	0.5	1000	0.05	N/A	1.0–1.5	[113]
	GPC-$FeNi_3$/S	1108	850	0.2	200	0.11	N/A	1.4–1.8	[116]
	Fe-Ni/S	1160	N/A	0.1	N/A	N/A	8	4.1	[117]
	S/Fe_2N@C	1129	881	1	600	0.036	13	1.1–4.1	[121]
	S/$FeSe_2$@C	~950[c]	684	1	700	0.04	15	1.5	[123]
	$Co_{5.47}N/Fe_3N$@N-CNT-G/S	~1293	N/A	0.1	500	0.029	7	2.7	[124]

[a] 1 C = 1675 mA/g.
[b] Electrolyte/sulfur ratio.
[c] Estimated initial discharge capacity since the specific value was not given in the reference.

To achieve high-performance Li-S battery, with splendid electrochemical performances, the safety and economic benefits are also needed to be considered. As a rising star, iron-based nanomaterial exhibits remarkable performance in Li-S battery. There is still a long way to go, yet, with the virtue of inherent advantages, more exciting achievements related to the mechanism and performance will be gained in the coming future.

Declaration of competing interest

The authors declare no conflict of interest.

Acknowledgments

This work was financially supported by National Natural Science Foundation of China (Nos. 51702362 and 21875282), Natural Science Foundation of Hunan Province (Nos. 2022JJ30663, 2022JJ40551) Scientific Research Project of National University of Defense Technology (No. ZK19–27), and Significant Independent Research Projects for Young Talents of College of Aerospace Science and Engineering, National University of Defense Technology.

References

[1] M. Li, J. Lu, Z.W. Chen, K. Amine, Adv. Mater. 30 (2018) 1800561.
[2] R.P. Fang, S.Y. Zhao, Z.H. Sun, et al., Adv. Mater. 29 (2017) 1606823.
[3] J. Balach, J. Linnemann, T. Jaumann, L. Giebeler, J. Mater. Chem. A 6 (2018) 23127–23168.
[4] S. Huang, E. Huixiang, Y. Yang, et al., J. Mater. Chem. A 9 (2021) 7458–7480.
[5] Y. Su, Y. Fu, T. Cochell, A. Manthiram, Nat. Commun. 4 (2013) 2985.
[6] D.R. Wang, D.B. Shah, J.A. Maslyn, et al., J. Electrochem. Soc. 165 (2018) A3487–A3495.
[7] M.R. Busche, P. Adelhelm, H. Sommer, et al., J. Power Sources 259 (2014) 289–299.
[8] Z. Seh, Y. Sun, Q. Zhang, Y. Cui, Chem. Soc. Rev. 45 (2016) 5605–5634.
[9] J. Xu, T. Lawson, H.B. Fan, et al., Adv. Energy Mater. 8 (2018) 1702607.
[10] J.J. Song, C.Y. Zhang, X. Guo, et al., J. Mater. Chem. A 6 (2018) 16610–16616.
[11] J.Y. Wu, X.W. Li, H.X. Zeng, et al., J. Mater. Chem. A 7 (2019) 7897–7906.
[12] Y.G. Cao, Q.A. Wu, Y.C. Chen, et al., J. Electrochem. Soc. 168 (2021) 070510.
[13] Y.Z. Song, H. Gao, M.L. Wang, et al., EcoMat 4 (2022) e12182.
[14] X.D. Hong, R. Wang, Y. Liu, et al., J. Energy Chem. 42 (2020) 144–168.
[15] D. Liu, C. Zhang, G. Zhou, et al., Adv. Sci. 5 (2018) 1700270.
[16] G. Babu, K. Ababtain, K.Y.S. Ng, L.M.R. Arava, Sci. Rep. 5 (2015) 8763.
[17] H. Al Salem, G. Babu, C.V. Rao, L.M.R. Arava, J. Am. Chem. Soc. 137 (2015) 11542–11545.
[18] Y. Yu, M. Yan, W.D. Dong, et al., Chem. Eng. J. 417 (2021) 129241.
[19] P.Y. Wang, R. Zeng, L. You, A.C.S. Appl, et al., Nano Mater. 3 (2020) 1382–1390.
[20] B. Guan, X. Sun, Y. Zhang, et al., Chin. Chem. Lett. 32 (2021) 2249–2253.
[21] J.H. Cheng, D. Zhao, L.S. Fan, et al., J. Mater. Chem. A 5 (2017) 14519–14524.
[22] S.L. Yu, W.L. Cai, L. Chen, et al., J. Energy Chem. 55 (2021) 533–548.
[23] A. Maurin, M. Robert, J. Am. Chem. Soc. 138 (2016) 2492–2495.
[24] Y.J. Sa, D.J. Seo, J. Woo, et al., J. Am. Chem. Soc. 138 (2016) 15046–15056.
[25] H.X. Zhang, S.F. Li, B. Zhao, et al., Chin. J. Inorg. Chem. 36 (2020) 1205–1222.
[26] M. Chen, E. Wang, Q. Liu, et al., Energy Storage Mater. 19 (2019) 163–178.
[27] C. Hao, T. Gao, A. Yuan, J. Xu, Chin. Chem. Lett. 32 (2021) 113–118.
[28] Y.F. Zheng, W.J. Feng, Int. J. Electrochem. Sci. 16 (2021) 210370.
[29] S.F. Jiang, S. Huang, M.J. Yao, et al., Chin. Chem. Lett. 31 (2020) 2347–2352.
[30] Q. Wang, H.Q. Zhao, B.Y. Li, et al., Chin. Chem. Lett. 32 (2021) 1157–1160.
[31] H. Bandal, K.K. Reddy, A. Chaugule, H. Kim, J. Power Sources 395 (2018) 106–127.
[32] C. Zheng, S.Z. Niu, W. Lv, et al., Nano Energy 33 (2017) 306–312.
[33] Y.R. Zhong, K.R. Yang, W. Liu, et al., J. Phys. Chem. C 121 (2017) 14222–14227.
[34] L.S. Fan, H.X. Wu, X. Wu, et al., Electrochim. Acta 295 (2019) 444–451.
[35] J. Li, Y.L. Xu, Y. Zhang, et al., J. Mater. Chem. A 8 (2020) 19544–19554.
[36] X. Chen, H. Peng, R. Zhang, et al., ACS Energy Lett. 2 (2017) 795–801.
[37] Y. Boyjoo, H. Shi, E. Olsson, et al., Adv. Energy Mater. 10 (2020) 2000651.
[38] C. Ma, Y.Q. Zhang, Y.M. Feng, et al., Adv. Mater. 33 (2021) 2100171.
[39] H. Li, D. Liu, X.X. Zhu, et al., Nano Energy 73 (2020) 104763.
[40] L. Zhang, P. Liang, X.L. Man, et al., J. Phys. Chem. Solids 126 (2019) 280–286.
[41] Q.W. Zeng, R.M. Hu, Z.B. Chen, J.X. Shang, Mater. Res. Express 6 (2019) 095620.
[42] J. Zhou, X. Liu, L. Zhu, et al., Joule 2 (2018) 2681–2693.
[43] J. Shen, X. Xu, J. Liu, et al., ACS Nano 13 (2019) 8986–8996.
[44] S.Z. Huang, Y.V. Lim, X.M. Zhang, et al., Nano Energy 51 (2018) 340–348.
[45] C.Y. Zhou, X.C. Li, H.L. Jiang, et al., Adv. Funct. Mater. 31 (2021) 2011249.
[46] Q. Liu, Y. Wang, Z. Hu, Z. Zhang, RSC Adv. 11 (2021) 3079–3095.
[47] W. Zang, Z. Kou, S.J. Pennycook, J. Wang, Adv. Energy Mater. 10 (2020) 1903181.
[48] H. Zhang, W. Zhou, X. Lu, et al., Adv. Energy Mater. 10 (2020) 2000882.
[49] C. Lu, R. Fang, X. Chen, Adv. Mater. 32 (2020) 1906548.
[50] H. Zhang, X.F. Lu, Z.P. Wu, X.W.D. Lou, ACS Central Sci. 6 (2020) 1288–1301.
[51] Y. Miao, Y. Zheng, F. Tao, et al., Chin. Chem. Lett. 2 (2022) 1450–1463.
[52] L. Lin, H. Li, C. Yan, et al., Adv. Mater. 31 (2019) 1903470.
[53] X. Xu, Z. Xia, X. Zhang, et al., Appl. Catal. B: Environ. 259 (2019) 118042.
[54] Y. Chen, S. Ji, S. Zhao, et al., Nat. Commun. 9 (2018) 5422.
[55] S.Y. Zhou, S. Yang, X.W. Ding, et al., ACS Nano 14 (2020) 7538–7551.
[56] D.R. Deng, R.M. Yuan, P.K. Yu, et al., Adv. Energy Mater. 11 (2021) 2101156.
[57] H.J. Peng, Z.W. Zhang, J.Q. Huang, et al., Adv. Mater. 28 (2016) 9551–9558.
[58] Z.Z. Liu, L. Zhou, Q. Ge, et al., ACS Appl. Mater. Interfaces 10 (2018) 19311–19317.
[59] M. Jiang, R.X. Wang, K.L. Wang, et al., Nanoscale 11 (2019) 15156–15165.
[60] Y.Z. Wang, D. Adekoya, J.Q. Sun, et al., Adv. Funct. Mater. 29 (2019) 1807485.
[61] C. Lu, Y. Chen, Y. Yang, X. Chen, Nano Lett. 20 (2020) 5522–5530.
[62] Y. Qiu, L.S. Fan, M.X. Wang, et al., ACS Nano 14 (2020) 16105–16113.
[63] Q.J. Shao, L. Xu, D.C. Guo, et al., J. Mater. Chem. A 8 (2020) 23772–23783.
[64] K. Zhang, Z.X. Chen, R.Q. Ning, et al., ACS Appl. Mater. Interfaces 11 (2019) 25147–25154.

[65] G.Q. Cao, Z.K. Wang, D. Bi, et al., Chem. Eur. J. 26 (2020) 10314–10320.
[66] H.L. Ye, J.G. Sun, S.L. Zhang, et al., ACS Nano 13 (2019) 14208–14216.
[67] T.Q. Zhang, Z. Chen, J.X. Zhao, Y.H. Ding, Diamond Relat. Mater. 90 (2018) 72–78.
[68] J. Li, Z. Niu, C. Guo, et al., J. Energy Chem. 54 (2021) 434–451.
[69] T. Zhou, W. Lv, J. Li, et al., Energy Environ. Sci. 10 (2017) 1694–1703.
[70] L. Zhang, P. Liang, H.B. Shu, et al., J. Colloid Interface Sci. 529 (2018) 426–431.
[71] H. Lin, R.C. Jin, A.L. Wang, et al., Ceram. Int. 45 (2019) 17996–18002.
[72] Y. Yang, W. Yuan, X. Zhang, et al., Renew. Sust. Energ. Rev. 127 (2020) 109884.
[73] S. Tanaka, Y.V. Kaneti, N.L.W. Septiani, et al., Small Methods 3 (2019) 1800512.
[74] J. Ma, X. Guo, Y. Yan, et al., Adv. Sci. 5 (2018) 1700986.
[75] M. Ding, S.Z. Huang, Y. Wang, et al., J. Mater. Chem. A 7 (2019) 25078–25087.
[76] Y. Jin, C.C. Zhao, Y.C. Lin, et al., J. Mater. Sci. Technol. 33 (2017) 768–774.
[77] K. Lu, H. Zhang, S.Y. Gao, et al., Adv. Funct. Mater. 29 (2019) 1807309.
[78] Y. Zhang, R. Gu, S. Zheng, et al., J. Mater. Chem. A 7 (2019) 21747–21758.
[79] X.R. He, Y.J. Zhang, L.F. Yang, et al., Acta Metall. Sin. Engl. Lett. 34 (2021) 410–416.
[80] X. Wang, K. Zhu, Y. Ju, et al., J. Magn. Magn. Mater. 489 (2019) 165432.
[81] H.Y. Pan, Z. Tan, H.H. Zhou, et al., J. Energy Chem. 39 (2019) 101–108.
[82] Y.G. Zhang, G.R. Li, J.Y. Wang, et al., Adv. Funct. Mater. 30 (2020) 9.
[83] W. Weng, J.X. Xiao, Y.J. Shen, et al., Angew. Chem. Int. Ed. 60 (2021) 24905–24909.
[84] K. Xie, Y. You, K. Yuan, et al., Adv. Mater. 29 (2017) 1604724.
[85] Z. Gao, Y. Schwab, Y.Y. Zhang, et al., Adv. Funct. Mater. 28 (2018) 1800563.
[86] H. Wei, E.F. Rodriguez, A.S. Best, et al., ACS Appl. Mater. Interfaces 11 (2019) 13194–13204.
[87] Y.Z. Wang, M. Li, L.C. Xu, et al., Chem. Eng. J. 358 (2019) 962–968.
[88] Z.S. Jin, M. Zhao, T.N. Lin, et al., Chem. Eng. J. 388 (2020) 124315.
[89] Y. Liu, X.C. Li, Y. Liu, et al., Chem. Eng. J. 382 (2020) 122858.
[90] Q. Dong, F.L. Zhang, S. Ji, et al., J. Alloys Compd. 877 (2021) 160286.
[91] S.Y. Gao, F. Xia, B.M. Li, et al., ACS Appl. Mater. Interfaces 13 (2021) 17791–17799.
[92] C.L. Song, Z.H. Li, M.Z. Li, et al., ACS Appl. Nano Mater. 3 (2020) 9686–9693.
[93] S.X. Wang, X.Y. Liu, H.H. Duan, et al., Chem. Eng. J. 415 (2021) 129001.
[94] Y.J. Zhang, J. Qu, Q.Y. Ji, et al., Carbon 155 (2019) 353–360.
[95] M.S. Garapati, R. Sundara, Electrochim. Acta 362 (2020) 137035.
[96] M. Zhang, Y. Guo, Y.H. Wei, et al., J. Mater. Chem. A 8 (2020) 18987–19000.
[97] X. Wang, H.M. Kim, Y. Xiao, Y.K. Sun, J. Mater. Chem. A 4 (2016) 14915–14931.
[98] Y. Shi, B. Zhang, Chem. Soc. Rev. 45 (2016) 1781 -1781.
[99] D. Yang, D. Bhattacharjya, S. Inamdar, et al., J. Am. Chem. Soc. 134 (2012) 16127–16130.
[100] Y.G. Zhang, Y.G. Wang, R.J. Luo, et al., Nanoscale Horiz 5 (2020) 530–540.
[101] Z.X. Zhao, R. Pathak, X.M. Wang, et al., Electrochim. Acta 364 (2020) 137117.
[102] M. Ma, L.Y. Cao, K. Yao, et al., ACS Sustain. Chem. Eng. 9 (2021) 5315–5321.
[103] H.D. Yuan, X.L. Chen, G.M. Zhou, et al., ACS Energy Lett. 2 (2017) 1711–1719.
[104] Z.S. Qiao, Y.G. Zhang, Z.H. Meng, et al., Adv. Funct. Mater. 31 (2021) 2100970.
[105] Y.J. Chen, S.Y. Liu, X.T. Yuan, et al., Carbon 167 (2020) 446–454.
[106] Y.J. Li, X.Q. Lei, Y.F. Yuan, et al., ACS Central Sci. 6 (2020) 1827–1834.
[107] S. Qi, B. Xu, V.T. Tiong, et al., Chem. Eng. J. 379 (2020) 122261.
[108] Q.T. Xu, J.C. Li, H.G. Xue, S.P. Guo, J. Power Sources 379 (2018) 41–52.
[109] S.S. Zhang, D.T. Tran, J. Mater. Chem. A 4 (2016) 4371–4374.
[110] X.Y. Li, S. Feng, M. Zhao, et al., Angew. Chem. Int. Ed. 61 (2022) e202114671.
[111] Z.P. Zeng, W. Li, X.J. Chen, et al., ACS Sustain. Chem. Eng. 8 (2020) 3261–3272.
[112] R.R. Li, H.J. Shen, E. Pervaiz, M.H. Yang, Chem. Eng. J. 404 (2021) 126462.
[113] A. Benitez, J. Amaro-Gahete, D. Esquivel, et al., Nanomaterials 10 (2020) 424.
[114] D. Capkova, M. Almasi, T. Kazda, et al., Electrochim. Acta 354 (2020) 136640.
[115] J. Yao, M. Zhang, G.D. Han, et al., Ceram. Int. 46 (2020) 24155–24161.
[116] L. Chen, L.W. Huang, G.J. Chen, et al., Chem. Eur. J. 26 (2020) 8926–8934.
[117] J.R. He, A. Bhargav, A. Manthiram, ACS Nano 15 (2021) 8583–8591.
[118] Z. Zhang, A.H. Shao, D.G. Xiong, et al., ACS Appl. Mater. Interfaces 12 (2020) 19572–19580.
[119] P. Zeng, C. Liu, X.F. Zhao, et al., ACS Nano 14 (2020) 11558–11569.
[120] M. Zhao, H.J. Peng, Z.W. Zhang, et al., Angew. Chem. Int. Ed. 58 (2019) 3779–3783.
[121] W.W. Sun, C. Liu, Y.J. Li, et al., ACS Nano 13 (2019) 12137–12147.
[122] Q. Zheng, X. Cheng, H. Li, Catalysts 5 (2015) 1079–1091.
[123] W.W. Sun, Y.J. Li, S.K. Liu, et al., Chem. Eng. J. 416 (2021) 129166.
[124] T.T. Nguyen, J. Balamurugan, H.W. Go, et al., Chem. Eng. J. 427 (2022) 131774.